Momentum-Based Balance Control

Sung-Hee Lee, KAIST; Andreas Hofmann, MIT; Ambarish Goswami, Honda

Introduction

0.1 What is momentum?

0.2 Humanoid robot model

A humanoid can be modeled as a set of $N+1$ links interconnected by N joints, of up to six degrees of freedom each, forming a tree-structure topology. The motion of the links are referenced to a fixed base (inertial frame) which is labeled 0 while the links are labeled from 1 through N. Numbering of the links may be done in any manner such that link i's predecessor toward the root (link 0), indicated by $p(i)$, is always less than i. Joints in the tree are numbered such that joint i connects link i to link $p(i)$. A coordinate frame is attached to each link to provide a reference for quantities associated with the link.

An $n_i \times 1$ vector $\dot{\boldsymbol{q}}_i$ relates the velocity of link i to the velocity of its predecessor, link $p(i)$, where n_i is the number of degrees of freedom at the joint connecting the two links. The free modes of the joint are represented by the $6 \times n_i$ matrix $\boldsymbol{\Phi}_i$, such that the spatial velocity of link i is given as follows:

$$\mathbf{v}_i = \begin{bmatrix} \boldsymbol{\omega}_i \\ \boldsymbol{v}_i \end{bmatrix} = {}^i\boldsymbol{X}_{p(i)}\, \mathbf{v}_{p(i)} + \boldsymbol{\Phi}_i\, \dot{\boldsymbol{q}}_i \,, \tag{1}$$

where $\boldsymbol{\omega}_i$ and $\boldsymbol{v}_i$ are the angular and linear velocities of link i, respectively, as referenced to the link coordinate frame. We will use spatial notation [1, 2] for describing rigid-body velocity, acceleration, inertia, etc., using 6D vectors and tensors. ${}^i\boldsymbol{X}_{p(i)}$ is a 6×6 spatial transform which transforms spatial motion vectors from $p(i)$ to i coordinates. The matrix $\boldsymbol{\Phi}_i$ depends on the type of joint [1]. For instance, $\boldsymbol{\Phi}_i = [0\,0\,1\,0\,0\,0]^T$ for a revolute joint with the rotation axis being aligned with the Z-axis.

In order to model a humanoid when in flight, one of the links is modeled as a floating base (typically the torso) and numbered as link 1. A fictitious six degree-of-freedom (DoF) joint is inserted between the floating base and fixed base. In this case, $\boldsymbol{\Phi}_1 = \mathbf{1}_{6\times 6}$ where $\mathbf{1}_{6\times 6}$ is the identity matrix. The total number of degrees of freedom in the humanoid is n where $n = \sum n_i$. Note that n includes the six degrees of freedom for the floating base.

The spatial transform ${}^i\boldsymbol{X}_{p(i)}$ may be composed from the position vector ${}^{p(i)}\boldsymbol{p}_i$ from the origin of coordinate frame $p(i)$ to the origin of i, and the 3×3 rotation matrix ${}^i\boldsymbol{R}_{p(i)}$ which transforms 3D vectors from coordinate frame $p(i)$ to i:

$${}^i\boldsymbol{X}_{p(i)} = \begin{bmatrix} {}^i\boldsymbol{R}_{p(i)} & \mathbf{0} \\ {}^i\boldsymbol{R}_{p(i)}\, \boldsymbol{S}({}^{p(i)}\boldsymbol{p}_i)^T & {}^i\boldsymbol{R}_{p(i)} \end{bmatrix} . \tag{2}$$

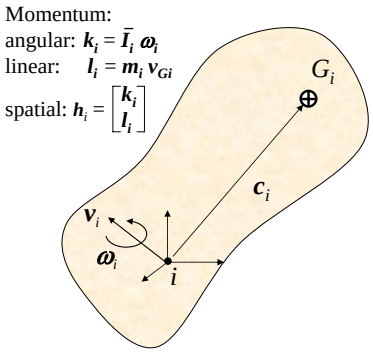

Fig. 1. Schematic depiction of a single rigid body: spatial momentum contains the angular and linear momenta.

The quantity $\boldsymbol{S}(\boldsymbol{p})$ is the skew-symmetric matrix that satisfies $\boldsymbol{S}(\boldsymbol{p})\,\boldsymbol{\omega} = \boldsymbol{p} \times \boldsymbol{\omega}$ for any 3D vector $\boldsymbol{\omega}$.

It is possible to combine the equations for the velocity or momentum for all the links into a global set of equations. To do so, composite vectors and matrices are defined. Global notation is useful in developing a system Jacobian which leads to an expression for the Centroidal Momentum Matrix.

Gathering all of the link velocities and joint velocities together, the system Jacobian $\boldsymbol{J}$ can be defined to give the relationship between the two:

$$\mathbf{v} = \boldsymbol{J}\,\dot{\boldsymbol{q}}\ , \tag{3}$$

where

$$\mathbf{v} = \left[\boldsymbol{v}_1^T,\, \boldsymbol{v}_2^T, \cdots \boldsymbol{v}_i^T, \cdots \boldsymbol{v}_N^T\right]^T\ . \tag{4}$$

The elements of the system Jacobian are just the Jacobians for each of the links:

$$\boldsymbol{J} = \left[\boldsymbol{J}_1^T,\, \boldsymbol{J}_2^T, \cdots \boldsymbol{J}_i^T, \cdots \boldsymbol{J}_N^T\right]^T\ . \tag{5}$$

0.3 Multibody system momenta

The spatial momentum of each link may be computed from the spatial velocity as follows (see Fig. 1):

$$\boldsymbol{h}_i = \begin{bmatrix} \boldsymbol{k}_i \\ \boldsymbol{l}_i \end{bmatrix} = \boldsymbol{I}_i\,\mathbf{v}_i\ , \tag{6}$$

where $\boldsymbol{k}_i$ is the angular momentum, $\boldsymbol{l}_i$ is the linear momentum, and $\boldsymbol{I}_i$ is the spatial inertia for link i. The spatial inertia may be composed from the mass m_i, position vector $\boldsymbol{c}_i$ to the center of mass (CoM) of link i, and 3×3 rotational inertia $\bar{\boldsymbol{I}}_i$, all relative to coordinate frame i:

$$\boldsymbol{I}_i = \begin{bmatrix} \bar{\boldsymbol{I}}_i & m_i\,\boldsymbol{S}(\boldsymbol{c}_i) \\ m_i\,\boldsymbol{S}(\boldsymbol{c}_i)^T & m_i\,\mathbf{1} \end{bmatrix}, \tag{7}$$

where

$$\bar{\boldsymbol{I}}_i = \bar{\boldsymbol{I}}_i^{cm} + m_i\,\boldsymbol{S}(\boldsymbol{c}_i)\,\boldsymbol{S}(\boldsymbol{c}_i)^T, \tag{8}$$

and $\bar{\boldsymbol{I}}_i^{cm}$ is the rotational inertia about the CoM. Recall that if the origin of coordinate frame i is chosen at the CoM, the off-diagonal blocks $m_i\,\boldsymbol{S}(\boldsymbol{c}_i)$ reduce to zero. If, in addition, the axes of coordinate frame i are oriented along the principal axes of inertia, $\bar{\boldsymbol{I}}_i$ becomes a 3×3 diagonal matrix and $\boldsymbol{I}_i$ a 6×6 diagonal matrix.

The momenta of all the links in the system may be determined as the product of the system velocity vector $\mathbf{v}$ and the system inertia $\boldsymbol{I}$; gathering all:

$$\boldsymbol{h} = \boldsymbol{I}\,\mathbf{v}\,, \tag{9}$$

where $\boldsymbol{h}$ is the $6N \times 1$ system momentum vector $\boldsymbol{h} = \left[\boldsymbol{h}_1^T,\, \boldsymbol{h}_2^T, \cdots \boldsymbol{h}_i^T, \cdots \boldsymbol{h}_N^T\right]^T$, and the $6N \times 6N$ system inertia matrix is defined as $\boldsymbol{I} = \mathrm{diag}\left[\boldsymbol{I}_1,\, \boldsymbol{I}_2, \cdots \boldsymbol{I}_i, \cdots \boldsymbol{I}_N\right]$.

0.4 Centroidal momentum

The aggregate momentum of a humanoid may be obtained by summing up all of the angular and linear momenta contributed by the individual link segments. As defined, the spatial momentum of each link $\boldsymbol{h}_i$ is most naturally expressed in its own coordinate system. As a measure of dynamic stability or for control, it is useful to combine the momenta for the links by projecting the momenta to a common coordinate frame. A convenient frame is one set at the instantaneous CoM or the centroid of the system G, and whose coordinate axes are parallel to those of the inertial coordinate frame 0. The 6×1 centroidal momentum vector $\boldsymbol{h}_G$, which consists of the linear and centroidal angular momenta of the robot, is the aggregate momentum with respect to the above-mentioned centroial frame. Noting that the spatial momentum may be projected as any other force-type vector [1], the following equation may be used to calculate the spatial momentum at the centroid of the system (see Fig. 2):

$$\boldsymbol{h}_G = \sum_{i=1}^{N} {}^i\boldsymbol{X}_G^T\,\boldsymbol{h}_i = \mathbf{X}_G^T\,\boldsymbol{h}\,, \tag{10}$$

where $\mathbf{X}_G$ is defined as the projection matrix, for motion vectors, from centroidal coordinates to link coordinates and is given as follows:

$$\mathbf{X}_G = \left[\,{}^1\boldsymbol{X}_G^T,\, {}^2\boldsymbol{X}_G^T,\, \cdots {}^i\boldsymbol{X}_G^T,\, \cdots {}^N\boldsymbol{X}_G^T\,\right]^T\,. \tag{11}$$

The centroidal momentum vector $\boldsymbol{h}_G$ is related to its $n \times 1$ joint velocity vector $\dot{\boldsymbol{q}}$ as:

$$\boldsymbol{h}_G = \boldsymbol{A}_G(\boldsymbol{q})\,\dot{\boldsymbol{q}}\,. \tag{12}$$

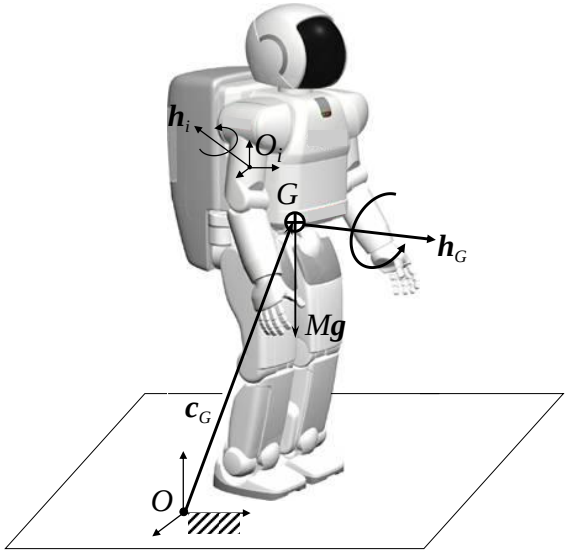

Fig. 2. Humanoid robot showing link and centroidal momentum vectors. The inertial frame is located at O and the position vector to the robot CoM, G, is given by $\boldsymbol{c}_G$. The reference frame of link i is located at O_i. The centroidal momentum $\boldsymbol{h}_G$ can be obtained from either Eq. 12 or Eq. 10.

The $6\times n$ matrix $\boldsymbol{A}_G$ is called the *Centroidal Momentum Matrix* and $\boldsymbol{A}_G$ contains contributions both from the inter-segmental joint variables of the robot as well as from the fictitious joint connecting the floating base of the humanoid to the inertial frame (detailed in Section 0.2). Note that $\boldsymbol{A}_G$ is identical to the large matrix in the RHS of Eq. 1 of [4], with only the linear and angular parts interchanged.

As shown in Eq. 12, the CMM gives the relationship between the joint rates and centroidal momentum. In order to find the relationship between this matrix and the link inertias and Jacobians, the concept of the *system momentum matrix* $\boldsymbol{A}$ is first presented. The system momentum matrix $\boldsymbol{A}$ expresses the relationship between the system momentum vector and the joint rates: $\boldsymbol{h} = \boldsymbol{A}\,\dot{\boldsymbol{q}}$.

Substituting the expression for the system velocity in Eq. 3 into Eq. 9, and using the definition of the system momentum matrix, we can write:

$$\boldsymbol{A} = \boldsymbol{I}\,\boldsymbol{J}\ . \tag{13}$$

The system momentum matrix is just the product of the system inertia matrix and the system Jacobian. It includes the momentum matrix for each link and is of size $6N \times n$:

$$\boldsymbol{A} = \left[\,\boldsymbol{A}_1^T,\ \boldsymbol{A}_2^T, \cdots \boldsymbol{A}_i^T, \cdots \boldsymbol{A}_N^T\,\right]^T\ , \tag{14}$$

with $\boldsymbol{A}_i = \boldsymbol{I}_i\,\boldsymbol{J}_i$.

The centroidal momentum may also be expressed as a function of the system momentum matrix $\boldsymbol{A}$:

$$\boldsymbol{h}_G = \mathbf{X}_G^T \boldsymbol{A}\, \dot{\boldsymbol{q}} \,. \tag{15}$$

Noting Eqs. 12 and 15, and using the expression for $\boldsymbol{A}$ in Eq. 13, the CMM, $\boldsymbol{A}_G$, may then be defined as:

$$\boldsymbol{A}_G = \mathbf{X}_G^T \boldsymbol{A} = \mathbf{X}_G^T \boldsymbol{I}\, \boldsymbol{J} \,, \tag{16}$$

which shows the relationship between $\boldsymbol{A}_G$ and the system inertia and Jacobian. Furthermore, time differentiation of Eq. 12 results in the following relation which forms the basis of our momentum-based balance controller presented later in this chatper:

$$\dot{\boldsymbol{h}}_G = \boldsymbol{A}_G\, \ddot{\boldsymbol{q}} + \dot{\boldsymbol{A}}_G\, \dot{\boldsymbol{q}} \,. \tag{17}$$

Finally, since $\mathbf{f} = \dot{\boldsymbol{h}}_G$ (Newton's equations of motion) where $\mathbf{f}$ is the net external force/moment on the system, then it may be noted that $\boldsymbol{A}_G$ gives the relationship between the net external force/moment and the joint accelerations.

0.5 Why momentum control is important

Until recently, most balance control techniques have attempted to maintain balance by controlling only the linear motion of a robot. For example, Kagami et al. [5] and Kudoh et al. [6] proposed methods to change the input joint angle trajectories to modify the position of the Center of Pressure (CoP), a point within the robot's support area through which the resultant Ground Reaction Force (GRF) acts. When the CoP, computed from the input joint motion, leaves the support base, indicating a possible toppling of a foot, the motion is modified to bring the CoP back inside the support base while the robot still follows the desired linear motion of the Center of Mass (CoM). The rotational motion of the robot remains more or less ignored in these approaches.

However, rotational dynamics of a robot plays a significant role in balance [7]. Experiments on human balance control also show that humans tightly regulate angular momentum during gait [8], which suggests the strong possibility that angular momentum may be important in humanoid movements.

In fact, both angular and linear momenta must be regulated to completely control the CoP. The fundamental quantities and the relations between them are schematically depicted in Fig. 3 and described subsequently.

Fig. 3(a) shows all the external forces that act on a freely standing humanoid: the GRF $\boldsymbol{f}$, the Ground Reaction Moment $\boldsymbol{\tau}_n$ normal to the ground, and the weight $m\boldsymbol{g}$ of the robot, where m is the total robot mass and $\boldsymbol{g}$ is the acceleration due to gravity. The sums of external moments and external forces are equivalent to the rates of change of angular and linear momenta, respectively, of the robot, and the mathematical expressions for these relationships are given by (18) and (19). Fig. 3(b) depicts the robot's rate of change of angular momentum about

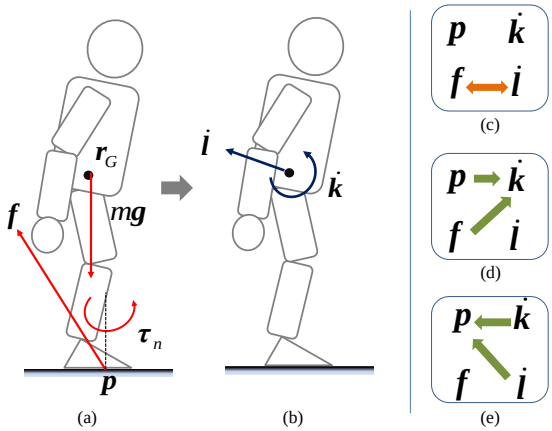

Fig. 3. The external forces and torques in (a) are solely responsible for the centroidal momentum rate change in (b). (c): Linear momentum rate change $\dot{\boldsymbol{l}}$ has a one-to-one correspondence with the GRF $\boldsymbol{f}$. (d): The centroidal angular momentum rate change $\dot{\boldsymbol{k}}$ is determined by both $\boldsymbol{f}$ and CoP location $\boldsymbol{p}$. (e): Conversely, $\boldsymbol{p}$ is determined by both $\dot{\boldsymbol{l}}$ and $\dot{\boldsymbol{k}}$.

the CoM, $\dot{\boldsymbol{k}}$, and linear momentum, $\dot{\boldsymbol{l}}$, respectively.

$$\dot{\boldsymbol{k}} = (\boldsymbol{p} - \boldsymbol{r}_G) \times \boldsymbol{f} + \boldsymbol{\tau}_n \tag{18}$$

$$\dot{\boldsymbol{l}} = m\boldsymbol{g} + \boldsymbol{f} \tag{19}$$

In the above equations, $\boldsymbol{r}_G$ is the CoM location and $\boldsymbol{p}$ is the CoP location. Together $\boldsymbol{k}$ and $\boldsymbol{l}$ is a 6×1 vector constitute the spatial centroidal momentum $\boldsymbol{h}_G = [\boldsymbol{k}^T \ \boldsymbol{l}^T]^T$. In this chapter, we will call it spatial momentum, or simply the momentum of the robot.

Indeed, as noted in [9], the (spatial) momentum rate change has a one-to-one relationship with the GRF and CoP. From (19) and as shown in Fig. 3(c), $\dot{\boldsymbol{l}}$ is completely determined by $\boldsymbol{f}$ and vice versa. Furthermore, from (18) and Fig. 3(d), a complete description of $\dot{\boldsymbol{k}}$ needs both $\boldsymbol{f}$ and $\boldsymbol{p}$. Conversely, $\boldsymbol{p}$ depends on both $\dot{\boldsymbol{k}}$ and $\dot{\boldsymbol{l}}$, which is shown in Fig. 3(e).[1] This last sentence implies that a complete control of $\boldsymbol{p}$ is impossible without controlling both momenta.

0.6 A word on ground reaction force

Related Work

[1] The normal torque $\boldsymbol{\tau}_n$ also affects $\dot{\boldsymbol{k}}$ in the transverse plane. Actually $\boldsymbol{f}$, $\boldsymbol{p}$, and $\boldsymbol{\tau}_n$ together constitute the 6 variables that correspond to the 6 variables of the spatial momentum. Usually $\boldsymbol{\tau}_n$ is omitted in the discussion for simplicity because its magnitude is small.

Starting from the early work of [10], researchers have developed numerous techniques for biped balance control using various approaches. Among these are joint control strategies using ankle or hip [11, 12], whole body control approaches [4, 5, 13–16], methods that find optimal control policies [17, 18], and reflex controllers [19]. In this section we focus on the research relevant to momentum-based balance control.

The importance of angular momentum in humanoid walking was reported by Sano and Furusho as early as 1990 [11]. However, it was much later before its importance for balance maintenance of human and humanoid robots started to be seriously explored [4, 8, 20]. Sano and Furusho [11], and Mitobe et al. [21] showed that it is possible to generate the desired angular momentum by controlling the ankle torque. Kajita et al. [4] included angular momentum criteria into the whole body control framework for balance maintenance. After expressing desired linear and angular momenta as linear functions of the generalized velocities, they determined the joint velocities that achieved both momenta.

Komura et al. [7] presented a balance controller that can counteract rotational perturbations using the Angular Momentum Pendulum Model (AMPM). This model augments the well known 3D Linear Inverted Pendulum Model (LIPM) [22] with the additional capability of possessing centroidal angular momentum. Naksuk et al. [23] proposed an iterative method to compute joint trajectories of humanoid robots to satisfy the desired CoM trajectory and to minimize the centroidal angular momentum. Other papers that deal with angular momentum for balance and gait include [24–28].

Abdallah and Goswami [29] defined balance control objectives in terms of CoM and CoP, and achieved this goal by controlling the rate of change of linear and angular momenta of a reduced model humanoid robot. The joint accelerations to generate the target momentum rate change were resolved using the Moore-Penrose pseudo-inverse.

Hofmann et al. [30] presented a method that controls CoM by modulating angular momentum under large external perturbations. It gives higher priority to controlling linear momentum over angular momentum to enhance the performance of the balance controller.

Table 1 illustrates how the existing methods treat momentum, GRF, and CoP in formulating balance and gait strategies. Robot gait planning methods using reduced models such as [14, 22] (Table 1 (a)) compute the necessary CoM trajectory which ensures balance for a specified desired CoP trajectory. This is done using reduced models such as the LIPM. As can be seen from Fig. 3(e) CoP depends on both linear and angular momenta rate changes, so CoM cannot be uniquely determined solely from CoP. This was possible in [14, 22] because the reduced model used in those works approximated the robot as a point mass, which can only possess a *zero* angular momentum.

In the Resolved Momentum Control approach [4], both desired linear and angular momenta are used to determine joint motion for posture change (Table 1 (b)). However, the admissibility of the CoP is not considered so the robot may lose balance if the values of input desired momenta are high. The methods

in Table 1 (c) determine the desired angular momentum rate change given desired CoP and linear momentum rate change. In our current method (Table 1 (d)), starting from the desired linear/angular momenta rate changes, we first determine admissible foot GRFs and CoPs, and then compute corresponding admissible momenta rate changes.

Table 1. The diagrams show how each method on balance control or gait pattern generation treats momenta ($\boldsymbol{k}, \boldsymbol{l}$), GRF ($\boldsymbol{f}$), and CoP ($\boldsymbol{p}$). A pair of solid lines determines the target value together. The dotted line shows the determination process of linear motion and force. The subscript "d" indicates a desired input to the controller and superscript "$*$" indicates that the quantity is used to determine control output such as joint torques.

(a) Kajita et al. [22], Choi et al. [14]	(b) Kajita et al. [4]	(c) Abdallah and Goswami [29], Macchhietto et al. [9]	(d) Lee and Goswami [31], [32]
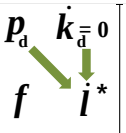	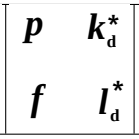	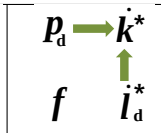	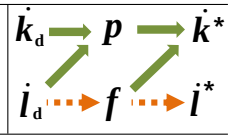

Ugurlu and Kawamura have studied bipedal walking that specifically controls the centroidal angular momentum [40]. Relatively recently we have seen a comprehensive study of angular momentum during human gait [41].

0.7 Comparison with ZMP-based control

Controller Formulation and Framework

Some momentum-based balance control approaches define the desired rotational behavior of the controller in terms of the CoP [9, 29] while others use angular momentum [4]. Although the GRF-CoP combination has a one-to-one relationship with momentum rate changes, their significance regarding balance are different: Whereas the former characterize the magnitude, direction and point of application of the external forces, the latter describes the resulting motion of a robot. The unilateral nature of robot-ground contact and friction limits impose important direct constraints on the range of GRF and CoP. These influence the achievable range of momentum rate change, but only indirectly. On the other hand, it is more natural to describe the aggregate motion of a robot in terms of momentum.

In this chapter we present a momentum-based balance controller developed in [32] that uses momentum to define control objectives as well as to compute joint motions while GRF and CoP are used as constraints. Fig. 4 shows the block

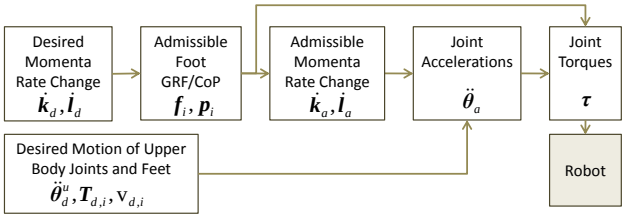

Fig. 4. Overview of momentum-based balance controller introduced in [32]. $\ddot{\boldsymbol{\theta}}_d^u$ is the desired joint accelerations for the upper body. $\mathbf{T}_{d,i}$ and $\mathbf{v}_{d,i}$ are the desired configuration and spatial velocity of each foot ($i = r, l$). Subscripts d and a imply *"desired"* and *"admissible,"* respectively.

diagram for the controller. In this method, the desired momentum rate change for balance is first specified. However, the desired momentum rate change may not always be physically realizable due to several constraints on the foot-ground contact. First, the CoP cannot be outside the robot's support base.[2] Second, the GRF must be unilateral in nature, and can never attract the robot towards the ground. Third, the GRF must satisfy the friction limit of the foot-ground surface, so as not to cause slip.

Therefore, the next step determines the admissible values of GRF and CoP that will create the desired momentum rate change as close as possible while being physically realizable. Specifically, in order to make the controller robustly applicable to non-level and non-stationary ground, admissible *foot* GRFs and *foot* CoPs ared directly determined, without using more conventional *net* GRF and *net* CoP of the robot. Assuming planar contact between the ground and each foot, the foot GRF is the ground reaction force acting on an individual foot and foot CoP is the location where its line of action intersects the foot support plane. Using the values of admissible foot GRF and foot CoP momentum rate changes are recalculated – these are the *admissible* momentum rate changes.

The subsequent step resolves the joint accelerations given the admissible momentum rate change, desired joint accelerations for the upper body, and desired motion of the feet. Finally necessary joint torques are computed to create the joint accelerations and the admissible external forces using inverse dynamics.

During double support, the computation of foot GRFs and foot CoPs from the desired momentum rate change is an under-determined problem. This allows for pursuing an additional optimality criterion in the solution. For example, the ankle torques can be minimized while generating the desired momentum rate change. Minimizing ankle torque is important because typically the ankle torque is more constrained than others in that it should not cause foot tipping.

[2] During single support, the support base is identical to the foot contact area, whereas during double support on level ground, the support base is equivalent to the convex hull of the support areas of the two feet.

Let us review the above framework in terms of the equations of motion of a robot. Assuming stationary ground, the constraint equations due to ground contacts and the joint space equations of motion of the robot are as follows:

$$\mathbf{0} = \mathbf{J}_c \dot{\boldsymbol{q}} \tag{20}$$

$$\boldsymbol{\tau} = \mathbf{H}\ddot{\boldsymbol{q}} + \mathbf{C}\dot{\boldsymbol{q}} + \boldsymbol{\tau}_g - \mathbf{J}_c^T \boldsymbol{f}_c \tag{21}$$

where $\boldsymbol{\tau} \in \mathbb{R}^n$ denotes the generalized forces, $\mathbf{H}$ is the joint space inertia matrix, $\mathbf{C}\dot{\boldsymbol{q}}$ includes Coriolis and centrifugal terms and $\boldsymbol{\tau}_g$ is the gravity torque. $\boldsymbol{f}_c$ is a vector representing external "constraint" forces from the ground, determined by foot GRFs and CoPs, and the Jacobian $\mathbf{J}_c \in \mathbb{R}^{c \times n}$ transforms $\boldsymbol{f}_c$ to the generalized forces. The number of constraint equations c depends on the nature of constraint at the foot-ground contact. For example, when both the linear and angular motion of the support foot are constrained due to foot-ground contact, $c = 6$ for single support and $c = 12$ for double support. In this case, $\mathbf{J}_c\dot{\boldsymbol{q}}$ denotes the linear and angular velocities of the support foot given $\dot{\boldsymbol{q}}$, and $\mathbf{0}$ in (20) denotes zero velocity of the support foot.

Since the robot base is free floating, the first six elements of $\boldsymbol{\tau}$ are zero, i.e., $\boldsymbol{\tau}^T = [\mathbf{0}^T \ \boldsymbol{\tau}_s^T]$. Hence, we can divide (21) into two parts, one corresponding to the base, denoted by the subscript 0, and the other, subscripted with s, for the joints. Then (20) and (21) are rewritten as follows:

$$\mathbf{0} = \mathbf{J}_c\ddot{\boldsymbol{q}} + \dot{\boldsymbol{J}}_c\dot{\boldsymbol{q}} \tag{22}$$

$$\mathbf{0} = \mathbf{H}_0\ddot{\boldsymbol{q}} + \mathbf{C}_0\dot{\boldsymbol{q}} + \boldsymbol{\tau}_{g,0} - \mathbf{J}_{c,0}^T\boldsymbol{f}_c \tag{23}$$

$$\boldsymbol{\tau}_s = \mathbf{H}_s\ddot{\boldsymbol{q}} + \mathbf{C}_s\dot{\boldsymbol{q}} + \boldsymbol{\tau}_{g,s} - \mathbf{J}_{c,s}^T\boldsymbol{f}_c \tag{24}$$

where (22) is the time derivative of (20).

The balance controller determines the control input $\boldsymbol{\tau}_s$ through the following steps:

- **Step 1**: foot GRFs and foot CoPs (hence $\boldsymbol{f}_c$) are computed from the desired momentum rate change.
- **Step 2**: joint accelerations $\ddot{\boldsymbol{q}}$ are determined such that they satisfy both (22) and (23). Actually, as will be explained in Sec. 0.14, instead of directly using (23), we use the centroidal momentum equation (17), which is equivalent to (23). In general, if the total number of robot DoFs is greater than or equal to $c + 6$, a solution to $\ddot{\boldsymbol{q}}$ exists.
- **Step 3**: the required joint torques $\boldsymbol{\tau}_s$ satisfying (24) are computed from $\boldsymbol{f}_c$ and $\ddot{\boldsymbol{q}}$ using an inverse dynamics algorithm.

Note that, by computing $\boldsymbol{f}_c$ and $\ddot{\boldsymbol{q}}$ first, we can use efficient linear-time algorithms for inverse dynamics in **Step 3**, without having to compute the joint space equations of motion (21) which have a quadratic time complexity.

0.8 Single Support

0.9 Double Support

0.10 Level and non-level surface

0.11 Arbitrary stationary surface

0.12 Moving surface (bus, moving walkway, boat)

0.13 Estimation of CM and reaction point movement state

Scenarios

0.14 Stationary Balance

In this section, we show how the momentum control framework introduced in Sec. 0.7 is employed to create stationary balance.

Determination of the Desired Momentum. The overall behavior of the robot against external perturbations is determined by the desired momentum rate change. For the stationary balance, the following feedback control policy can be used:

$$\dot{\boldsymbol{k}}_d = \boldsymbol{\Gamma}_{11}(\boldsymbol{k}_d - \boldsymbol{k}) \tag{25}$$

$$\dot{\boldsymbol{l}}_d/m = \boldsymbol{\Gamma}_{21}(\dot{\boldsymbol{r}}_{G,d} - \dot{\boldsymbol{r}}_G) + \boldsymbol{\Gamma}_{22}(\boldsymbol{r}_{G,d} - \boldsymbol{r}_G) \tag{26}$$

where $\dot{\boldsymbol{k}}_d$ and $\dot{\boldsymbol{l}}_d$ are the independently specified desired rates of change of centroidal angular and linear momenta. In other words $\dot{\boldsymbol{k}}_d$ and $\dot{\boldsymbol{l}}_d$ are not time derivatives of $\boldsymbol{k}_d$ and $\boldsymbol{l}_d$. Additionally, $\boldsymbol{r}_{G,d}$ is the desired CoM position. $\boldsymbol{\Gamma}_{ij}$ represents 3×3 diagonal matrix of feedback gain parameters. Note that unlike the linear position feedback term in (26), an angular position feedback is omitted in (25). This is because a physically meaningful angular "position" cannot be defined corresponding to angular momentum [43]. For postural balance maintenance experiments we set $\boldsymbol{k}_d$ and $\dot{\boldsymbol{r}}_{G,d}$ to zero and $\boldsymbol{r}_{G,d}$ to be above the mid-point of the geometric centers of the two feet. For other cases, these values may be determined from the desired motion.

It is to be noted that, despite the various studies on angular momentum in humanoid motions, the issue of how to set the desired angular momentum for more complex motions such as locomotion has not been fully explored, and remains an important future work.

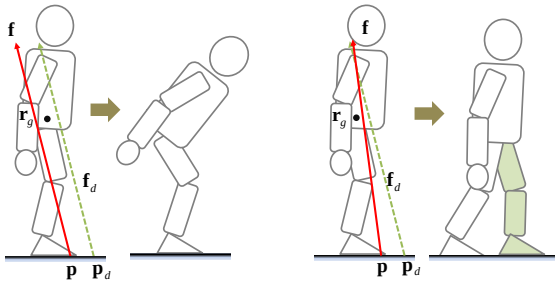

Fig. 5. When the desired GRF, $\boldsymbol{f}_d$ and the desired CoP, $\boldsymbol{p}_d$ computed from the desired momentum rate change are not simultaneously admissible, as indicated by $\boldsymbol{p}_d$ being outside the support base, momenta objectives need to be compromised for control law formulation. Two extreme cases are illustrated. Left: linear momentum is respected while angular momentum is compromised. Right: angular momentum is respected while linear momentum is compromised.

Prioritization between Linear and Angular Momenta Given the desired momentum rate change, admissible foot GRF and foot CoP are determined such that the resulting momentum rate change is as close as possible to the desired value. If the desired GRF and CoP computed from $\dot{\boldsymbol{k}}_d$ and $\dot{\boldsymbol{l}}_d$ violate physical constraints (e.g., GRF being outside friction cone, normal component of GRF being negative, or CoP being outside support base), it is not possible to generate those $\dot{\boldsymbol{k}}_d$ and $\dot{\boldsymbol{l}}_d$. In this case we must strike a compromise and decide which quantity out of $\dot{\boldsymbol{k}}_d$ and $\dot{\boldsymbol{l}}_d$ is more important to preserve.

Fig. 5 illustrates one case where the desired CoP, $\boldsymbol{p}_d$, computed from the desired momentum rate change is outside the support base, indicating that it is not admissible. Two different solutions are possible. The first solution, shown in Fig. 5, left, is to translate the CoP to the closest point of the support base while keeping the magnitude and line of action of the desired GRF $\boldsymbol{f}_d$ unchanged. In this case the desired linear momentum is attained but the desired angular momentum is compromised. The behavior emerging from this choice is characterized by a trunk rotation. This strategy can be observed in the human when the trunk yields in the direction of the push to maintain balance. Alternatively, in addition to translating the CoP to the support base, as before, we can rotate the direction of the GRF, as shown in Fig. 5, right. In this case the desired angular momentum is attained while the desired linear momentum is compromised. With this strategy the robot must move linearly along the direction of the applied force due to the residual linear momentum, making it necessary to step forward to prevent falling.

For the stationary balance, it is natural to give higher priority to preserving linear momentum over angular momentum because it increases the capability of postural balance without involving a stepping. Ideally, a smart controller should be able to choose optimal strategies depending on the environment conditions

and the status of the robot. The approaches that give higher priority to linear momentum and sacrifice angular momentum can also be found in the literature [16, 30] and in our recent work on stepping [44].

Admissible Foot GRF, Foot CoP, and Momentum Rate Change. Given the desired momentum rate change, admissible foot GRF and CoP are determined such that the resulting momentum rate change is as close as possible to the desired value. Admissible momentum rate change is determined by the admissible foot GRF and foot CoP.

Single Support Case: Dealing with single support case is straightforward because the foot GRF and CoP are uniquely determined from the desired momentum rate change, from (18) and (19):

$$\boldsymbol{f}_d = \dot{\boldsymbol{l}}_d - m\boldsymbol{g} \tag{27}$$

$$p_{d,X} = r_{G,X} - \frac{1}{\dot{l}_{d,Y} - mg}(f_{d,X}\, r_{G,Y} - \dot{k}_{d,Z}) \tag{28}$$

$$p_{d,Z} = r_{G,Z} - \frac{1}{\dot{l}_{d,Y} - mg}(f_{d,Z}\, r_{G,Y} + \dot{k}_{d,X}) \tag{29}$$

where the Y-axis is parallel to the direction of gravity vector, i.e., $\boldsymbol{g} = (0, g, 0)$.

If $\boldsymbol{f}_d$ and $\boldsymbol{p}_d$ computed above are valid, then these values are directly used. Otherwise, as mentioned previously, higher priority is given to linear momentum. If $\boldsymbol{f}_d$ is outside the friction cone, it is projected onto the friction cone to prevent foot slipping.

Double Support Case: Determining foot GRFs and foot CoPs for double support is more involved. Let us first rewrite (18) and (19) for the double support case. Following [11], we will express the GRF at each foot in terms of the forces and torques *applied to the corresponding ankle* (Fig. 6). The benefit of this representation is that we can explicitly express the torques applied to the ankles.

$$\dot{\boldsymbol{k}} = \dot{\boldsymbol{k}}_f + \dot{\boldsymbol{k}}_\tau \tag{30}$$

$$\dot{\boldsymbol{k}}_f = (\boldsymbol{r}_r - \boldsymbol{r}_G) \times \boldsymbol{f}_r + (\boldsymbol{r}_l - \boldsymbol{r}_G) \times \boldsymbol{f}_l \tag{31}$$

$$\dot{\boldsymbol{k}}_\tau = \boldsymbol{\tau}_r + \boldsymbol{\tau}_l \tag{32}$$

$$\dot{\boldsymbol{l}} = m\boldsymbol{g} + \boldsymbol{f}_r + \boldsymbol{f}_l \tag{33}$$

In (30), we have divided $\dot{\boldsymbol{k}}$ into two parts, $\dot{\boldsymbol{k}}_f$, due to the ankle force, and $\dot{\boldsymbol{k}}_\tau$, due to ankle torque. This division enables us to take ankle torques into account in determining foot GRFs. $\boldsymbol{f}_r$ and $\boldsymbol{f}_l$ are the GRFs at the right and left foot, respectively, and $\boldsymbol{r}_r$, $\boldsymbol{r}_l$ are the positions of the body frames of the foot, located at the respective ankle joints.

The ankle torques $\boldsymbol{\tau}_i$, $(i = r, l)$ are expressed in terms of foot GRF and foot CoP as follows (Fig. 7):

$$\boldsymbol{\tau}_i = (\mathbf{R}_i \boldsymbol{d}_i) \times \boldsymbol{f}_i + \mathbf{R}_i \boldsymbol{\tau}_{n,i}\,, \tag{34}$$

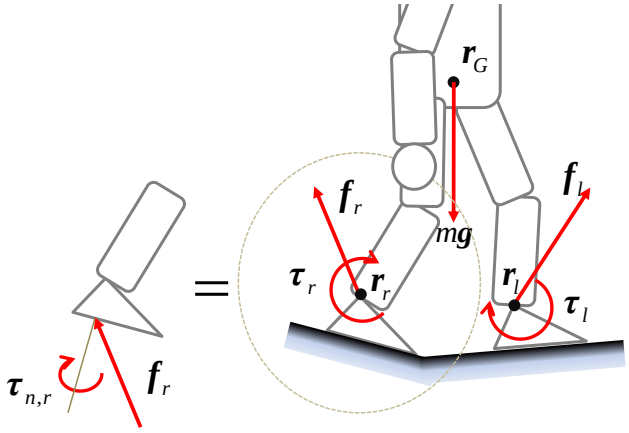

Fig. 6. By expressing GRF applied to each foot with respect to the local frame of the foot located at the ankle, we can factor out the moments $\boldsymbol{\tau}_r$, $\boldsymbol{\tau}_l$ applied to the ankle by the foot GRFs $\boldsymbol{f}_r$ and $\boldsymbol{f}_l$. $\boldsymbol{r}_r$ and $\boldsymbol{r}_l$ are the positions of the ankles.

where $\mathbf{R}_i$ is the orientation of the foot, $\boldsymbol{d}_i$ is the foot CoP in body frame, and $\boldsymbol{\tau}_{n,i} = (0, 0, \tau_{n,i})$ is the normal torque in body frame.

Given $\dot{\boldsymbol{k}}$ and $\dot{\boldsymbol{l}}$, solving for foot GRFs and foot CoPs is an underdetermined problem, which lets us prescribe additional optimality criteria to find a solution. If we incorporate minimal ankle torques into the optimality condition, we could express the objective function as follows:

$$\begin{aligned} w_l||\dot{\boldsymbol{l}}_d - \dot{\boldsymbol{l}}(\boldsymbol{f}_r, \boldsymbol{f}_l)||^2 + w_k||\dot{\boldsymbol{k}}_d - \dot{\boldsymbol{k}}(\boldsymbol{f}_r, \boldsymbol{f}_l, \boldsymbol{\tau}_r, \boldsymbol{\tau}_l)||^2 \\ + w_f\left(||\boldsymbol{f}_r||^2 + ||\boldsymbol{f}_l||^2\right) + w_\tau\left(||\boldsymbol{\tau}_r||^2 + ||\boldsymbol{\tau}_l||^2\right) \\ \text{s.t. } \boldsymbol{f}_i \text{ and } \boldsymbol{\tau}_i \text{ are admissible} \end{aligned} \tag{35}$$

where the first two terms aim to achieve the desired momentum rate change, the third term regularizes foot GRFs, and the last term tries to minimize ankle torques. w's are weighting factors among the different objectives.

Equation (35) represents a nonlinear and non-quadratic optimization problem and it especially contains nonlinear cross product terms (see (34)); this makes it difficult to use in a real-time controller. One solution is to convert this general nonlinear optimization problem to easier ones that can be solved using least-squares or quadratic programming methods. This can be achieved by expressing the foot GRF and foot CoP using the forces at certain specific locations on the boundary of the foot soles [45,46]. However, this approach increases the dimension of the search space significantly. Instead of increasing the search space to make the optimization problem easier, we approximate (35) with two constrained least-squares problems, one for determining the foot GRFs, and the other for determining the foot CoPs. This way the number of variables is kept

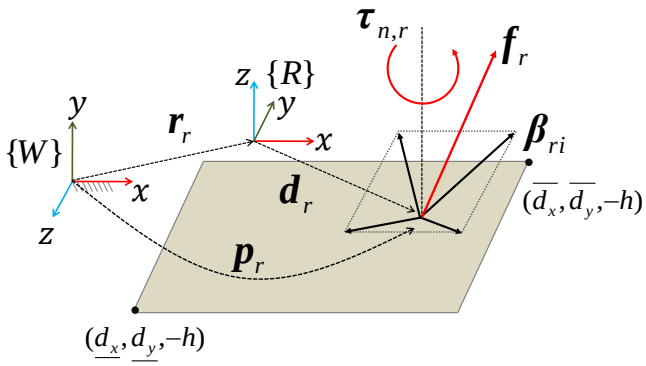

Fig. 7. We represent the foot/ground interaction forces on the right foot using foot CoP, whose location with respect to the right foot frame $\{R\}$ is denoted by $\boldsymbol{d}_r = (\boldsymbol{d}_{r,X}, \boldsymbol{d}_{r,Y}, -h)$, ground reaction moment normal to the ground $\boldsymbol{\tau}_{n,r} = (0, 0, \tau_{n,r})$, and the GRF $\boldsymbol{f}_r$.

small. Additionally, we attempt to minimize the ankle torques. Minimizing ankle torques is meaningful because large ankle torques can cause foot slipping.

This approach can be intuitively understood as follows. In order to minimize the ankle torques ($\dot{\boldsymbol{k}}_\tau \rightarrow \boldsymbol{0}$), the foot GRFs $\boldsymbol{f}_r$ and $\boldsymbol{f}_l$ should create $\dot{\boldsymbol{k}}_f$ as close to the desired angular momentum rate change ($\dot{\boldsymbol{k}}_f \rightarrow \dot{\boldsymbol{k}}_d$) as possible while satisfying $\dot{\boldsymbol{l}}_d$. If $\dot{\boldsymbol{k}}_f = \dot{\boldsymbol{k}}_d$, the ankle torques can vanish. If $\dot{\boldsymbol{k}}_f \neq \dot{\boldsymbol{k}}_d$, we compute the ankle torques that are necessary to generate the residual angular momentum rate change, $\dot{\boldsymbol{k}}_d - \dot{\boldsymbol{k}}_f$. In other words, by reducing burdens on the ankle torques to create $\dot{\boldsymbol{k}}_d$, it solves (35) for the case in which minimizing ankle torques has higher priority than regularizing foot GRFs.

Determination of Foot GRFs: In order to compute the foot GRFs, $\boldsymbol{f}_r$ and $\boldsymbol{f}_l$, we solve the optimization problem below:

$$\begin{aligned} \min ||\dot{\boldsymbol{l}}_d - \dot{\boldsymbol{l}}(\boldsymbol{f}_r, \boldsymbol{f}_l)||^2 + w_k ||\dot{\boldsymbol{k}}_d - \dot{\boldsymbol{k}}_f(\boldsymbol{f}_r, \boldsymbol{f}_l)||^2 \\ + \epsilon_f (||\boldsymbol{f}_r||^2 + ||\boldsymbol{f}_l||^2) \,, \end{aligned} \tag{36}$$

where w_k and ϵ_f ($w_k \gg \epsilon_f > 0$) are weighting factors for angular momentum and the regularization of foot GRFs, respectively. Note that, if $\dot{\boldsymbol{k}}_d = \dot{\boldsymbol{k}}_f$, the ankle torques $\boldsymbol{\tau}_i$ become zero. Each foot GRF is modeled using four basis vectors $\boldsymbol{\beta}_{ij}$ and their magnitudes ρ_{ij} that approximate the friction cone (an inverted pyramid in Fig. 7) on the ground

$$\boldsymbol{f}_i = \sum_{j=1}^{4} \boldsymbol{\beta}_{ij} \rho_{ij} := \boldsymbol{\beta}_i \boldsymbol{\rho}_i \,, \tag{37}$$

where $\boldsymbol{\beta}_i = [\boldsymbol{\beta}_{i1} \ \cdots \ \boldsymbol{\beta}_{i4}]$.

Note that $\boldsymbol{r}_r$ and $\boldsymbol{r}_l$ are determined by the configuration of the robot; they are constants when solving this problem. Therefore $\dot{\boldsymbol{k}}_f$ becomes a linear equation of $\boldsymbol{\rho}_i$ when we substitute (37) into (31). Rearranging into a matrix equation, we can turn the optimization problem (36) into a linear least-squares problem with non-negativity constraints where the only unknowns are the $\boldsymbol{\rho}_i$:

$$\min ||\boldsymbol{\Phi}\boldsymbol{\rho} - \boldsymbol{\xi}||^2 \text{ s.t. } \boldsymbol{\rho}_i \geq 0\,, \tag{38}$$

where [3]

$$\boldsymbol{\Phi} = \begin{bmatrix} \boldsymbol{\beta}_r & \boldsymbol{\beta}_l \\ w_f\boldsymbol{\delta}_r & w_f\boldsymbol{\delta}_l \\ \epsilon_f\mathbf{1} & \end{bmatrix} \in \mathbb{R}^{(3+3+8)\times(4+4)} \tag{39}$$

$$\boldsymbol{\xi} = \begin{bmatrix} \dot{\boldsymbol{l}}_d - m\boldsymbol{g} \\ w_f\dot{\boldsymbol{k}}_d \\ \mathbf{0} \end{bmatrix} \in \mathbb{R}^{(3+3+8)}$$

$$\boldsymbol{\rho} = \begin{bmatrix} \boldsymbol{\rho}_r^T & \boldsymbol{\rho}_l^T \end{bmatrix}^T \in \mathbb{R}^8 \tag{40}$$

$$\boldsymbol{\delta}_i = [\boldsymbol{r}_i - \boldsymbol{r}_G]_\times \boldsymbol{\beta}_i \tag{41}$$

Determination of Foot CoPs: In general, the desired angular momentum rate change cannot be fully generated only by $\boldsymbol{f}_r$ and $\boldsymbol{f}_l$, so the residual, $\dot{\boldsymbol{k}}_{\tau,d} = \dot{\boldsymbol{k}}_d - \dot{\boldsymbol{k}}_f$, should be generated by the ankle torques. To this end, we determine the location of each foot CoP such that they create $\dot{\boldsymbol{k}}_{\tau,d}$ while minimizing each ankle torque. It is to be noted that, after having determined $\boldsymbol{f}_i$, (34) can be written as a linear function of $\boldsymbol{d}_i$ and $\boldsymbol{\tau}_{n,i}$:

$$\boldsymbol{\tau}_i = -[\boldsymbol{f}_i]_\times \mathbf{R}_i\boldsymbol{d}_i + \mathbf{R}_i\boldsymbol{\tau}_{n,i}\,, \tag{42}$$

so that we can express the optimization problem as a least-squares problem with upper and lower bounds:

$$\min ||\boldsymbol{\Psi}\boldsymbol{\eta} - \boldsymbol{\kappa}||^2 \text{ s.t. } \underline{\boldsymbol{\eta}} \leq \boldsymbol{\eta} \leq \overline{\boldsymbol{\eta}}\,, \tag{43}$$

where

$$\boldsymbol{\Psi} = \begin{bmatrix} \boldsymbol{\Psi}_k \\ \epsilon_p\mathbf{1} \end{bmatrix} \in \mathbb{R}^{(3+6)\times 6},\ \boldsymbol{\kappa} = \begin{bmatrix} \boldsymbol{\kappa}_k \\ \epsilon_p\boldsymbol{\eta}_d \end{bmatrix} \in \mathbb{R}^{(3+6)} \tag{44}$$

$$\boldsymbol{\eta} = [d_{r,X}\ d_{r,Y}\ \tau_{n,r}\ d_{l,X}\ d_{l,Y}\ \tau_{n,l}]^T \in \mathbb{R}^6\,, \tag{45}$$

[3] The vector $\boldsymbol{\delta}_i$ expresses angular momentum rate change (31) in terms of $\boldsymbol{\rho}_i$ as follows:

$$(\boldsymbol{r}_r - \boldsymbol{r}_G) \times \boldsymbol{f}_r = (\boldsymbol{r}_r - \boldsymbol{r}_G) \times (\boldsymbol{\beta}_r\boldsymbol{\rho}_r) = \underbrace{[\boldsymbol{r}_i - \boldsymbol{r}_G]_\times \boldsymbol{\beta}_r}_{\boldsymbol{\delta}_r}\boldsymbol{\rho}_r := \boldsymbol{\delta}_r\boldsymbol{\rho}_r$$

where the elements of the constant matrix $\boldsymbol{\Psi}_k \in \mathbb{R}^{3\times 6}$ and $\boldsymbol{\kappa}_k$ are determined from (42).[4]

$\underline{\boldsymbol{\eta}}$ and $\overline{\boldsymbol{\eta}}$ are determined from foot geometry, friction coefficient, and the normal component of foot GRF (see Fig. 7). $\boldsymbol{\eta}_d$ is chosen such that $\boldsymbol{\tau}_i$ is zero, i.e., the line of action of $\boldsymbol{f}_i$ intersects the ankle. Note that both the least-squares problems have a small number of variables, so the optimization can be carried out quickly.

Admissible Momentum Rate Change After determining admissible foot GRF and foot CoP, the admissible momentum rate change $\dot{\boldsymbol{h}}_a = [\dot{\boldsymbol{k}}_a^T \ \dot{\boldsymbol{l}}_a^T]^T$ is also computed using (18) and (19) for single support, or (30) and (33) for double support.

Determination of Joint Accelerations and Torques After determining the admissible foot GRFs and foot CoPs, and admissible momentum rate changes, we compute joint accelerations and torques to realize them similarly to [9].

Specifically, we compute the output accelerations of the balance controller $\ddot{\boldsymbol{\theta}}$ such that they minimize the following objective function:

$$\begin{aligned} \ddot{\boldsymbol{\theta}}_a = \underset{\ddot{\boldsymbol{\theta}}}{\operatorname{argmin}} \ & w_b||\dot{\boldsymbol{h}}_a - \mathbf{A}\ddot{\boldsymbol{q}} - \dot{\boldsymbol{A}}\dot{\boldsymbol{q}}|| + (1-w_b)||\ddot{\boldsymbol{\theta}}_d^u - \ddot{\boldsymbol{\theta}}^u|| \\ & \text{s.t. } \mathbf{J}\ddot{\boldsymbol{q}} + \dot{\boldsymbol{J}}\dot{\boldsymbol{q}} = \boldsymbol{a}_d \quad \text{and} \quad \ddot{\boldsymbol{\theta}}_l \le \ddot{\boldsymbol{\theta}} \le \ddot{\boldsymbol{\theta}}_u \,, \end{aligned} \tag{46}$$

where $\dot{\boldsymbol{h}}_a$ is the admissible momentum rate change. We will call the output acceleration vector the admissible acceleration, and denote it by $\ddot{\boldsymbol{\theta}}_a$. Note that $\ddot{\boldsymbol{\theta}}_a$ contains all the joint accelerations except those of the floating joints. Because there can be infinitely many solutions for $\ddot{\boldsymbol{\theta}}_a$ that create $\dot{\boldsymbol{h}}_a$, we have an additional optimality criteria in (46), which is to follow the desired joint acceleration of the upper body $\ddot{\boldsymbol{\theta}}_d^u$ as closely as possible. One can set $\ddot{\boldsymbol{\theta}}_d^u$ to specify an upper-body task, or set $\ddot{\boldsymbol{\theta}}_d^u = \mathbf{0}$ to minimize the movement. The parameter $w_b (0 < w_b < 1)$ controls the relative importance between the balance objective (the first term) and the prescribed motion objective associated with the kinematic task (the second term). It is to be noted that w_b should be close to 1 in order to create admissible momentum rate, but it cannot be exactly 1 because in this case (46) becomes indeterminate. $\boldsymbol{a}_d = [\boldsymbol{a}_{d,r}^T \ \boldsymbol{a}_{d,l}^T]^T$ is the desired accelerations of the right and left feet. Section 0.14 details how to determine $\boldsymbol{a}_d$. Equation (46) can

[4] Specifically, $\boldsymbol{\Psi}_k = [\boldsymbol{\Psi}_k^0 \dots \boldsymbol{\Psi}_k^5]$ where

$$\begin{aligned} \boldsymbol{\Psi}_k^0 &= -\mathbf{R}_r^1 \boldsymbol{f}_{r,Z}^b + \mathbf{R}_r^2 \boldsymbol{f}_{r,Y}^b, \quad \boldsymbol{\Psi}_k^1 = \mathbf{R}_r^0 \boldsymbol{f}_{r,Z}^b - \mathbf{R}_r^2 \boldsymbol{f}_{r,X}^b, \quad \boldsymbol{\Psi}_k^2 = \mathbf{R}_r^2, \\ \boldsymbol{\Psi}_k^3 &= -\mathbf{R}_l^1 \boldsymbol{f}_{l,Z}^b + \mathbf{R}_l^2 \boldsymbol{f}_{l,Y}^b, \quad \boldsymbol{\Psi}_k^4 = \mathbf{R}_l^0 \boldsymbol{f}_{l,Z}^b - \mathbf{R}_l^2 \boldsymbol{f}_{l,X}^b, \quad \boldsymbol{\Psi}_k^5 = \mathbf{R}_l^2, \end{aligned}$$

and $\boldsymbol{\kappa}_k = \dot{\boldsymbol{k}}_{\tau,d} + h(\mathbf{R}_r^1 \boldsymbol{f}_{r,X}^b - \mathbf{R}_r^0 \boldsymbol{f}_{r,Y}^b + \mathbf{R}_l^1 \boldsymbol{f}_{l,X}^b - \mathbf{R}_l^0 \boldsymbol{f}_{l,Y}^b)$. $\mathbf{R}_i^j$ is j-th column vector of $\mathbf{R}_i$ $(i = r, l)$, $\boldsymbol{f}_i^b = \mathbf{R}_i^T \boldsymbol{f}_i$, and h is the height of foot frame from the foot sole.

be easily converted to a least-squares problem with linear equality and bound constraints, and many solvers (e.g., [48]) are available for this type of problem.

We set $\ddot{\boldsymbol{\theta}}_l$ and $\ddot{\boldsymbol{\theta}}_u$, the lower and upper bound of the joint accelerations, somewhat heuristically such that the joint limit constraints are satisfied (e.g., $\ddot{\boldsymbol{\theta}}_u$ decreases when a joint angle approaches its upper limit).

Finally, we compute the feedforward torque input $\boldsymbol{\tau}_{ff}$ from $\ddot{\boldsymbol{\theta}}_a$ and the admissible external forces by performing inverse dynamics. Since external forces are explicitly specified for the support feet by (38) and (43) and joint accelerations are set by (46), we have all the necessary information for inverse dynamics. Specifically, we use the hybrid system dynamics algorithms [2], which is useful for performing inverse dynamics for floating-base mechanisms.

Overall torque input is determined by adding feedback terms:

$$\boldsymbol{\tau}_s = \boldsymbol{\tau}_{ff} + \boldsymbol{\tau}_{fb} \tag{47}$$

$$\boldsymbol{\tau}_{fb} = \boldsymbol{\Gamma}_p(\boldsymbol{\theta}^* - \boldsymbol{\theta}) + \boldsymbol{\Gamma}_d(\dot{\boldsymbol{\theta}}^* - \dot{\boldsymbol{\theta}})\,, \tag{48}$$

where $\boldsymbol{\Gamma}_p = \mathrm{diag}(\gamma_{p,i})$ and $\boldsymbol{\Gamma}_d = \mathrm{diag}(\gamma_{d,i})$ are proportional and derivative gains, respectively. Position and velocity commands $\boldsymbol{\theta}^*$, $\dot{\boldsymbol{\theta}}^*$ are determined from the time integration of $\ddot{\boldsymbol{\theta}}_a$.

Desired Motion of the Feet We set the desired foot accelerations $\boldsymbol{a}_d$ such that each foot has the desired configuration $\mathbf{T}_d \in \mathrm{SE}$ and velocity $\mathbf{v}_d \in \mathrm{se}$. Specifically, for each foot, we use the following feedback rule:

$$\boldsymbol{a}_{d,i} = k_p \log(\mathbf{T}_i^{-1}\mathbf{T}_{d,i}) + k_d(\mathbf{v}_{d,i} - \mathbf{v}_i)\,, \tag{49}$$

for $i \in \{r, l\}$ where k_p and k_d are proportional and derivative feedback gains, respectively. The $\log : \mathrm{SE} \to \mathrm{se}$ function computes the twist coordinates corresponding to a transformation matrix [49]. The current configuration $\mathbf{T}$ and velocity $\mathbf{v}$ of a foot can be computed from the forward kinematics operation assuming that the robot can either measure or estimate the joint angles and velocities as well as the configuration and velocity of the trunk, e.g., from an accelerometer and a gyroscope.

0.15 Push Recovery and Stepping

Synchronization

0.16 Relation to biological control (ankle and hip strategies)

Controller Optimality

0.17 Angular momentum reservoir limits

Discussion and Open Questions

0.18 Principled prioritization between linear and angular momenta

0.19 Balance during tipping

——————— Outline recommended in template ———————

Synonyms

- Synonym 1
- Synonym 2
- ...

List only acronyms and those words with exactly the same meaning. All words that appear as synonyms will be directly linked back to the home entry, with no additional information given.

Related Concepts

- Related concept 1
- Related concept 2
- ...

This includes keywords. All related concepts will point to other entries in the encyclopedia.

Definition

One or two sentences summarizing the concept of the entry.

Background

Describe the background of the entry.

Theory or Application, or Both

Describe the theory (application) of the entry. It can be either Theory or Application, or it could be both of them.

Open problems (optional)

Describe the new trends, unsolved problems related to the entry.

Experimental Results (optional)

Experimental results that help the understandings of the entry. It can be videos, codes, etc.

Recommended Readings

[1] R. Featherstone and D. E. Orin. Dynamics, chapter 2. *Springer Handbook of Robotics, B. Siciliano and O. Khatib, Eds.*, 2008.

[2] Roy Featherstone. *Robot Dynamics Algorithms*. Kluwer Academic Publishers, 1987.

[3] A. Jain G. Rodriguez and K. Kreutz-Delgado. A spatial operator algebra for manipulator modelling and control. *Intn'l J. of Robotics Research*, 10(4):371–381, 1991.

[4] S. Kajita, F. Kanehiro, K. Kaneko, K. Fujiwara, K. Harada, K. Yokoi, and H. Hirukawa. Resolved momentum control: Humanoid motion planning based on the linear and angular momentum. In *IEEE/RSJ Intn'l Conf. on Intelligent Robots and Systems (IROS)*, volume 2, pages 1644–1650, 2003, Las Vegas, NV, USA.

[5] S. Kagami, F. Kanehiro, Y. Tamiya, M. Inaba, and H. Inoue. AutoBalancer: An online dynamic balance compensation scheme for humanoid robots. In *Proc. of the 4th International Workshop on Algorithmic Foundation on Robotics*, 2000.

[6] S. Kudoh, T. Komura, and K. Ikeuchi. The dynamic postural adjustment with the quadratic programming method. In *IEEE/RSJ Intn'l Conf. on Intelligent Robots and Systems (IROS)*, 2002.

[7] T. Komura, H. Leung, S. Kudoh, and J. Kuffner. A feedback controller for biped humanoids that can counteract large perturbations during gait. In *IEEE Intn'l Conf. on Robotics and Automation (ICRA)*, pages 2001–2007, 2005, Barcelona, Spain.

[8] M. Popovic, A. Hofmann, and H. Herr. Angular momentum regulation during human walking: Biomechanics and control. In *IEEE Intn'l Conf. on Robotics and Automation (ICRA)*, pages 2405–2411, April, New Orleans, LA, USA 2004.

[9] Adriano Macchietto, Victor Zordan, and Christian R. Shelton. Momentum control for balance. *ACM Transactions on Graphics*, 28(3):80:1–80:8, July 2009.

[10] M. Vukobratović and D. Juričić. Contribution to the synthesis of biped gait. *IEEE Trans. Bio-Medical Eng.*, 16(1), 1969.

[11] A. Sano and J. Furusho. Realization of natural dynamic walking using the angular momentum information. In *IEEE Intn'l Conf. on Robotics and Automation (ICRA)*, pages 1476 – 1481, May 1990.

[12] Benjamin Stephens. Integral control of humanoid balance. In *IEEE/RSJ Intn'l Conf. on Intelligent Robots and Systems (IROS)*, 2007.

[13] T. Sugihara, Y. Nakamura, and H. Inoue. Realtime humanoid motion generation through ZMP manipulation based on inverted pendulum control. In *IEEE Intn'l Conf. on Robotics and Automation (ICRA)*, pages 1404–1409, May 2002.

[14] Youngjin Choi, Doik Kim, Yonghwan Oh, and Bum-Jae You. Posture/walking control for humanoid robot based on kinematic resolution of CoM Jacobian with embedded motion. *IEEE Trans. on Robotics*, 23(6):1285–1293, 2007.

[15] Jonghoon Park, Youngil Youm, and Wan-Kyun Chung. Control of ground interaction at the zero-moment point for dynamic control of humanoid robots. In *IEEE Intn'l Conf. on Robotics and Automation (ICRA)*, pages 1724 – 1729, April 2005.

[16] Benjamin J. Stephens and Christopher G. Atkeson. Dynamic balance force control for compliant humanoid robots. In *IEEE/RSJ Intn'l Conf. on Intelligent Robots and Systems (IROS)*, 2010.

[17] Changjiu Zhou and Qingchun Meng. Dynamic balance of a biped robot using fuzzy reinforcement learning agents. *Fuzzy Sets and Systems*, 134(1):169–187, 2003.

[18] Uldarico Muico, Yongjoon Lee, Jovan Popović, and Zoran Popović. Contact-aware nonlinear control of dynamic characters. *ACM Transactions on Graphics*, 28(3), 2009.

[19] Qiang Huang and Yoshihiko Nakamura. Sensory reflex control for humanoid walking. *IEEE Trans. on Robotics*, 21(5):977–984, Oct. 2005.

[20] A. Goswami and V. Kallem. Rate of change of angular momentum and balance maintenance of biped robots. In *IEEE Intn'l Conf. on Robotics and Automation (ICRA)*, pages 3785–3790, April 2004.

[21] K. Mitobe, G. Capi, and Y. Nasu. A new control method for walking robots based on angular momentum. *Mechatronics*, 14(2):163–174, 2004.

[22] S. Kajita, F. Kanehiro, K. Kaneko, K. Yokoi, and H. Hirukawa. The 3D linear inverted pendulum model: A simple modeling for a biped walking pattern generator. In *IEEE/RSJ Intn'l Conf. on Intelligent Robots and Systems (IROS)*, pages 239–246, 2001, Maui, Hawaii.

[23] N. Naksuk, Y. Mei, and C.S.G. Lee. Humanoid trajectory generation: an iterative approach based on movement and angular momentum criteria. In *IEEE/RAS Intn'l Conf. on Humanoid Robots*, pages 576–591, Nov. 2004.

[24] N. E. Sian, K. Yokoi, S. Kajita, F. Kanehiro, and K. Tanie. Whole body teleoperation of a humanoid robot -a method of integrating operator??s intention and robot's autonomy. In *IEEE Intn'l Conf. on Robotics and Automation (ICRA)*, 2003.

[25] Kyung-Ho Ahn and Yonghwan Oh. Walking control of a humanoid robot via explicit and stable CoM manipulation with the angular momentum resolution. In *IEEE/RSJ Intn'l Conf. on Intelligent Robots and Systems (IROS)*, 2006.

[26] Barkan Ugurlu and Atsuo Kawamura. Eulerian ZMP resolution based bipedal walking: Discussions on the rate change of angular momentum about center of mass. In *IEEE Intn'l Conf. on Robotics and Automation (ICRA)*, 2010.

[27] Yuting Ye and C. Karen Liu. Optimal feedback control for character animation using an abstract model. *ACM Transactions on Graphics*, 29(3), 2010.

[28] Martin de Lasa, I. Mordatch, and A. Hertzmann. Feature-based locomotion controllers. *ACM Transactions on Graphics*, 29(3), 2010.

[29] M. Abdallah and A. Goswami. A biomechanically motivated two-phase strategy for biped robot upright balance control. In *IEEE Intn'l Conf. on Robotics and Automation (ICRA)*, pages 3707–3713, April 2005, Barcelona, Spain.

[30] Andreas Hofmann, Marko Popovic, and Hugh Herr. Exploiting angular momentum to enhance bipedal center-of-mass control. In *IEEE Intn'l Conf. on Robotics and Automation (ICRA)*, pages 4423–4429, May 2009.

[31] Sung-Hee Lee and Ambarish Goswami. Ground reaction force control at each foot: A momentum-based humanoid balance controller for non-level and non-stationary ground. In *IEEE/RSJ Intn'l Conf. on Intelligent Robots and Systems (IROS)*, 2010.

[32] Sung-Hee Lee and Ambarish Goswami. A momentum-based balance controller for humanoid robots on non-level and non-stationary ground. *Autonomous Robots*, 33(4):399–414, 2012.

[33] Yasutaka Fujimoto and Atsuo Kawamura. Simulation of an autonomous biped walking robot including environmental force interaction. *IEEE Robotics & Automation Magazine*, 5(2):33–41, 1998.

[34] Yasutaka Fujimoto, Satoshi Obata, and Atsuo Kawamura. Robust biped walking with active interaction control between foot and ground. In *IEEE Intn'l Conf. on Robotics and Automation (ICRA)*, pages 2030–2035, 1998.

[35] Yasutaka Fujimoto. *Study on Biped Walking Robot with Environmental Force Interaction*. PhD thesis, Yokohama National University, 1998.

[36] L. Sentis, J. Park, and O. Khatib. Compliant control of multicontact and center-of-mass behaviors in humanoid robots. *IEEE Trans. on Robotics*, 26(3):483–501, 2010.

[37] J. Park, J. Han, and F.C. Park. Convex optimization algorithms for active balancing of humanoid robots. *IEEE Trans. on Robotics*, 23(4):817–822, 2007.

[38] Tomomichi Sugihara and Yoshihiko Nakamura. Variable impedant inverted pendulum model control for a seamless contact phase transition on humanoid robot. In *IEEE-RAS/RSJ International Conference on Humanoid Robots*, 2003.

[39] Tomomichi Sugihara. *Mobility Enhancement Control of Humanoid Robot based on Reaction Force Manipulation via Whole Body Motion*. PhD thesis, University of Tokyo, 2003.

[40] B. Ugurlu and A. Kawamura. Eulerian zmp resolution based bipedal walking: Discussion on the intrinsic angular momentum rate change about center of mass. In *IEEE Intn'l Conf. on Robotics and Automation (ICRA)*, pages 4218–4223, 2010.

[41] H. Herr and M. Popovic. Angular momentum in human walking. *The Journal of Experimental Biology*, 211:467–481, 2008.

[42] A. M. Bloch, P. S. Krishnaprasad, J. E. Marsden, and R. M. Murray. Nonholonomic mechanical systems with symmetry. *Archive for Rational Mechanics and Analysis*, 136(1):21–99, Dec. 1996.

[43] P.-B. Wieber. Holonomy and nonholonomy in the dynamics of articulated motion. In *Fast Motions in Biomechanics and Robotics, Heidelberg, Germany*, Heidelberg, Germany 2005.

[44] S-K. Yun and A. Goswami. Momentum-based reactive stepping controller on level and non-level ground for humanoid robot push recovery. In *IEEE/RSJ Intn'l Conf. on Intelligent Robots and Systems (IROS)*, September 2011.

[45] Nancy S. Pollard and Paul S. A. Reitsma. Animation of humanlike characters: Dynamic motion filtering with a physically plausible contact model. In *Yale Workshop on Adaptive and Learning Systems*, 2001.

[46] Sang-Ho Hyon, J.G. Hale, and G. Cheng. Full-body compliant human–humanoid interaction: Balancing in the presence of unknown external forces. *IEEE Trans. on Robotics*, 23(5):884–898, 2007.

[47] D. Orin and A. Goswami. Centroidal momentum matrix of a humanoid robot: Structure and properties. In *IEEE/RSJ Intn'l Conf. on Intelligent Robots and Systems (IROS)*, 2008, Nice, France.

[48] M.I.A. Lourakis. levmar: Levenberg-marquardt nonlinear least squares algorithms in C/C++. [web page] `http://www.ics.forth.gr/~lourakis/levmar/`, Jul. 2004.

[49] Richard M. Murray, Zexiang Li, and S. Shankar Sastry. *A Mathematical Introduction to Robotic Manipulation*. CRC Press, 1994.